2013 IEEE/RSJ International Conference on
Intelligent Robots and Systems (IROS)
November 3-7, 2013. Tokyo, Japan

Conically Shaped Remote Center-of-Motion Mechanism for Single-Incision Surgery

Hyundo Choi, Hyung Joo Kim, Yo-An Lim, Ho-Seong Kwak, Jun-Won Jang, and Jonghwa Won

Abstract—**In this paper, we introduce a remote center-of-motion (RCM) mechanism with a conical shape for laparoscopic surgeries that involve a single incision. The mechanism, which has two revolute joints and one prismatic joint, is designed to maintain a stationary point at the apex of the conical shape. By aligning the stationary point with the incision area, the mechanism allows a surgical instrument to explore the abdominal area through a small incision point. We have previously analyzed the reachable workspace of this mechanism. Here, we arrange two RCM mechanisms on a single conical structure but separated in space to avoid mutual interference, so as to enable the entire system to manipulate two surgical instruments through a single incision point without colliding. We describe the operational principle of this system, in addition to comparisons of various RCM mechanisms and the kinematics for parameter design and motion control. Finally, we describe preliminary experiments on peg transfer and suture motion by using the proposed RCM mechanism.**

I. Introduction

A. Single-Incision Laparoscopic Surgery

Single-incision laparoscopic surgery (SILS), or single-port access (SPA) surgery, is a recently developed laparoscopic procedure that involves passing multiple instruments and an endoscope through a single incision [1][2]. It is a minimally invasive surgical procedure in which the surgeon operates almost exclusively through a single entry point, typically the patient's navel. When compared with traditional multi-port laparoscopic techniques, the benefits of SILS techniques include less postoperative pain, less blood loss, faster recovery time, and better cosmetic results.

Despite the potential advantages of SILS techniques, there may also be limitations such as inadequate triangulation and an impaired view at positions in line with the instrument [3]. Additionally, the small operation space can make it difficult to manipulate surgical instruments and an endoscope because they are passed through a single incision. These problems can be solved by the improved ergonomic design, accuracy, and dexterity provided by teleoperated robotic surgery systems. Many researchers have attempted to apply robotics technologies to SILS.

A number of manual single-site surgeries have been successfully performed by adopting an endoscopic robot [4][5]. The aim of these studies was to substitute a robotic manipulating system for the assistant surgeon tasked with manipulating the endoscope. These studies efficiently overcame space limitations of the operation site. Many other robotic devices are currently being developed to address the dexterity and visualization limitations for SILS and to improve tissue manipulation capabilities as well as internal organ visualization.

The authors are with the Samsung Advanced Institute of Technology, San 14, Nongseo-dong, Giheung-gu, Yongin-si, Gyeonggi-do, Korea. (e-mail: hyundo.choi@samsung.com; hjuro.kim@samsung.com; yoan.lim@samsung.com; hoseong.kwak@samsung.com; jw526.jang@samsung.com; jhwon@samsung.com).

B. Related Work and Research Aim

In one approach, robotics technologies have been applied to instruments as well as endoscopes. In this approach, the surgery area is accessed by an overtube that includes the surgical instruments and endoscope, and surgery is performed locally. Examples include a bimanual robotic system with two arms having six degrees of freedom (DoFs) for single-port laparoscopy [6], or that with a deployable mechanical structure and stereo vision [7][8]. Master-slave robotic systems that use long flexible instruments with multiple DoFs alongside existing flexible endoscopes are currently being developed [9][10]. These overtube-type surgery robots have a single robotic arm that manipulates an overtube outside the patient's body. A surgeon can efficiently perform small-part surgery because the surgical instruments and endoscope are deployed from the same overtube, which can be flexible or rigid. However, view-independent instrument motion is limited by the overtube, and flexible overtubes can also degrade the stiffness of the instrument end. These problems can be more serious when multi-DoF motions of the instrument and endoscope must be implemented inside the body.

Another approach for single-site surgery involves substituting the surgeon's hand with a robotic arm; the rigid instruments and endoscope are connected to a robotic arm outside of the body and passed through the single incision. In particular, a remote center-of-motion (RCM) mechanism can be used to maintain the stationary point at the incision area. The *da Vinci* system from Intuitive Surgical has been used to improve surgical dexterity for performing transumbilical single-port radical prostatectomy, dismembered pyeloplasty, and right-side radical nephrectomy procedures [11]. Instruments modified for triangulation are also used in single-incision surgery performed with the *da Vinci* system [12]. An instrument that possesses high stiffness can be applied with relatively high force to the tissue and manipulated in a large workspace. However, existing surgical robot systems are not optimized to a single-port configuration, owing to collisions between the robotic arms that manipulate the surgical instruments and endoscope [13].

Recently, a more compact system to position and manipulate the surgical instruments has been proposed conceptually. The system is composed of two instruments and one endoscope attached to a common rotating base ring [14]. In this approach, the key requirements are to maintain triangulation of the instrument and to prevent mutual interference between the robotics arms.

A manipulator with redundant DoFs can also be substituted for a surgeon's hand, and pivoting motions can be generated by control algorithms for multiple joints [15][16]. These manipulators have advantages such as changeable pivot location and increased maneuverability. For surgical applications, however, mechanical RCMs are considered safer owing to their reduced DoFs, decoupled motion, controller simplicity, and locked pivot features [17]. In addition, RCM mechanisms, which can be lighter and more compact because of lower occupancy by actuators and actuation mechanisms, reduce the likelihood of interference between the robotic arms in single-site surgery.

In this paper, we propose an RCM mechanism that can prevent interference between the robotic arms by separating the areas of motion for single-port surgery when they are passed through a single incision. Most RCM mechanisms proposed to date have been designed for operating endoscopic cameras, percutaneous needles, and surgical instruments [18]. These designs have not considered the requirements of inserting multiple instruments and an endoscope into a single incision.

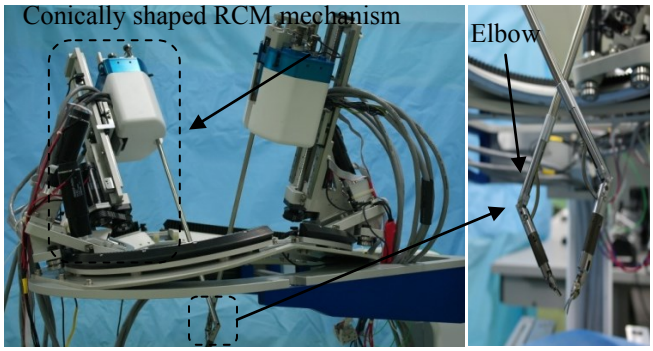

Figure 1. Single-incision surgery robot equipped with conically shaped RCM mechanism

The proposed mechanism is inspired by the work of [19], which described a compact modular robot for multi-port laparoscopic surgery that implements the RCM mechanism near incision areas. In this approach, the base frame, which stays stationary during surgery, is close to the incision area. Thus, the moving component of the mechanism is more compact than a system in which the base frame is far from the incision area.

Building upon this work, we designed the proposed conically shaped RCM mechanism to have a base frame near a single incision point. We successfully applied the proposed RCM mechanism to a surgical robot (Fig. 1) and showed that it could prevent mechanical interference between the robotic arms during peg transfer and suturing tests.

II. Remote Center-of-motion Mechanisms

In this section, we briefly describe the different types of RCM mechanism mentioned in [18] and consider their applicability to a single-incision surgery robot.

Nine different types of RCM mechanism, including the proposed mechanism, are presented in Table 1. We analyzed the previously proposed RCM mechanisms from the viewpoints of applicability, compactness, and results from implementation in SILS robots. To be applicable to SILS robots, an RCM mechanism should not have mechanical components such as linkages or joints around the incision area because the instruments and endoscope must pass through a single incision area. For compactness, a mechanism in which the base frame is close to an incision point was considered more compact than other mechanisms because the moving components of the mechanism must cover the distance from the base frame to the incision point (e.g., compact MIS robot RAVEN [29]). Finally, we investigated the RCM mechanisms that were implemented in SILS robots.

TABLE I. RCM Mechanisms and Applicability to SILS Robot

RCM Type	***Kinematic structure***	***Applicability to SILS robot***	***Ref.***
Isocenter	Revolute joint + Revolute joint	N, L	[20]
Circular tracking arc	Revolute joint + Circular track	A, L	[21]
Parallelogram	Parallel mechanism with several bars	**A, L, I**	[11] [22] [23]
Belt	Body-fixed pulley + Rotating linkage	A, L	[24]
Spherical linkage	Revolute joint + Revolute joint + Curved frame	**A, S**	[25]
Gimbal	Revolute joint + Revolute joint +Crossing axis	N, S	[26]
Parallel wrist	3 prismatic joints + 6 spherical joints	N, S	[27]
Gear train	Concentric revolute joint + Concentric revolute joint	**A, S**	[28]
Conical shape	Circular track + Revolute joint + Prismatic joint	**A, S, I**	

A: Applicable to SILS robot, **N**: Not applicable to SILS robots

S: Short distance between base frame and incision point, **L**: Long distance between the same

I: Implemented in SILS robots

The parallelogram-type mechanism is the most widely used RCM mechanism in the area of endoscope control, instrument manipulation, and needle insertion [11][22]. The *da Vinci* system [23], which is a successful example that has adopted a parallelogram-type RCM mechanism, is also implemented in SILS robots. The compactly designed RAVEN, which is from the University of Washington [29] and is based on a spherical linkage-type mechanism, is also a successful example of a minimally invasive surgical robot. However, it has not yet been applied to SILS robots. Isocenter, gimbal, and parallel wrist-type RCM mechanisms can be used for a single instrument or endoscope. However, they are not applicable to SILS, which requires instruments and endoscopes to pass through the same incision point.

As shown above, most research on RCM mechanisms has focused on applications to endoscope operation, needle insertion, and minimally invasive multi-port surgery. RCM mechanisms for SILS robots have not yet been actively studied.

III. Design of Conically Shaped RCM Mechanism

A. Requirements and approach

Some issues regarding the RCM mechanism should be considered before proceeding to its conceptual and detailed design. Considering the requirements of a single-port surgical procedure and referring to [18], which reviewed kinematic

design considerations for minimally invasive robots, we established the design goals (DGs) of the RCM mechanism. Table II presents these DGs and approaches to meet the goals.

TABLE II. DESIGN GOALS AND APPROACHES

	Design Goal	Approach
DG1	RCM constraint at the incision point	Circular track, Revolute joint, and Prismatic joint
DG2	High payload	Base frame close to an incision point
DG3	Large workspace	Parametric study
DG4	Collision-free motion of each robotic arm	Separation of motion area
DG5	Avoidance of mechanical interference 50 mm around a single incision	Proper positioning of two instruments (8 mm) and one endoscope (15 mm)

B. Operational Principle

The conceptual design of the proposed RCM mechanism is shown in Fig. 2. The mechanism consists of a base frame, an inner cone, an inner rotator, and a linear instrument guide. The base frame is fixed to the ground and the inner cone is connected to the base frame by a circular track, whose rotation axis passes through an apex of the conical structure of the base frame. The circular track can increase the stiffness of the mechanism because the inner rotator is supported by 4 points separated from one another. The inner rotator and inner cone are connected by a long revolute joint, whose rotation axis crosses the axis of the circular track. Thus, the point of intersection between the first and second axes becomes a stationary point. By using a prismatic joint attached between the inner rotator and instrument guide, an instrument can be passed through the intersection point. Finally, the two axes of the revolute joints and the axis of the prismatic joint converge at one point, which becomes the incision point in a surgery.

The joints that make up the conically shaped RCM mechanism are the circular track, a long revolute joint, and a prismatic joint. This novel and simple kinematic structure satisfies the DGs. The RCM constraint is satisfied when the three axes intersect at a single point (DG1). The mechanism with high stiffness can maintain high externally applied forces because the base frame is close to the incision point (DG2). In addition, the four supporting points of the circular track and long revolute joint prevent bending of the structure.

To prevent collisions of the instruments, the motion areas of the instrument guides are separated so that each covers half of the entire cone area (DG4). The remote centers of the two RCM mechanisms are also separated from one another while the two instrument guides are extended in opposite directions. This configuration enables collision-free motion of the RCM mechanisms and places instruments in triangulation positions. Interference between the arms is thus prevented in the design and simulation processes, and the robot can move freely in a given range of motion.

C. Kinematic Analysis

In this section, we derive the kinematic relations among the joint parameters and elbow position in Cartesian coordinates. Figure 2 shows the parameters of the proposed RCM mechanism, where γ and η are design variables and $\{\mathbf{a_1}\ \mathbf{a_2}\ \mathbf{a_3}\}$ is an inertial reference frame fixed to the ground. To account for the three joints that constitute the mechanism, the joint parameters are defined as $\boldsymbol{q} = [q_1\ q_2\ q_3]$, where q_1 is the rotation angle of the circular track, q_2 is the rotation angle of the long revolute joint, and q_3 is the displacement of the prismatic joint. By defining the position of the elbow as $\mathbf{p_e}$, we can write the forward kinematic relation of $\mathbf{p_e}$ and $\boldsymbol{q}$ as follows:

$$\mathbf{p}_e = \mathbf{\Phi(q)} \quad . \tag{1}$$

By using the rotation matrix with respect to the current rotation axis, we can rewrite equation (1) as follows:

$$\begin{aligned}\mathbf{p}_e &= \mathbf{R}_{\mathbf{a}_3,q_1}\mathbf{R}_{\mathbf{a}_1,\gamma}\mathbf{R}_{\mathbf{a}_2,q_2}\mathbf{R}_{\mathbf{a}_1,\eta}(-q_3\mathbf{c}_2) \\ &= -q_3\begin{pmatrix} c_1s_2s_\eta - s_1(c_\gamma c_\eta - s_\gamma s_\eta) \\ s_1s_2s_\eta - c_1(c_\gamma c_\eta - s_\gamma s_\eta) \\ s_\gamma c_\eta + c_\gamma s_\eta c_2 \end{pmatrix}.\end{aligned} \tag{2}$$

where c and s are abbreviations for cosine and sine, respectively, and subscripts *1* and *2* refer to q_1 and q_2, respectively. With a given set of joint parameters (q_1, q_2, q_3), we can calculate the elbow position. By using the forward kinematic relation, we analyzed the range and isotropy of the elbow workspace and determined the design values for γ and η. These issues will be discussed the following sections.

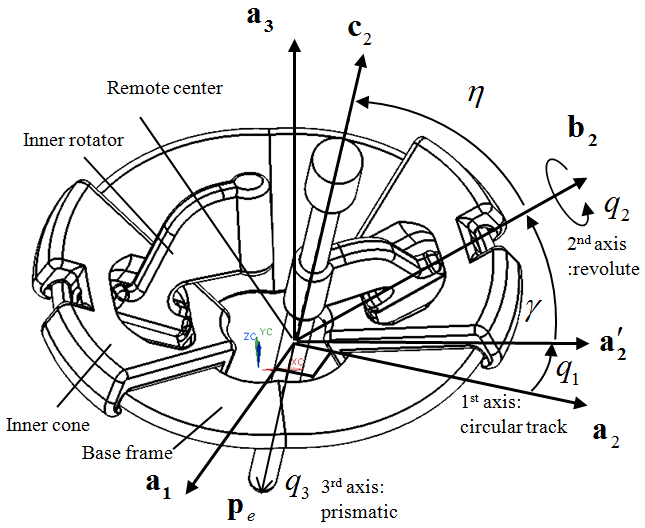

Figure 2. Conceptual design and parameter definition of the conically shaped RCM mechanism

The reverse relation, known as the inverse kinematics, is also derived in this section. From the inverse kinematics, we can find the reference control parameters of the joints given the desired elbow position. The inverse kinematic relation can be written as follows:

$$\mathbf{q} = \mathbf{\Phi}^{-1}(\mathbf{p}_e). \tag{3}$$

The RCM is located at (0 0 0) and the coordinate frames attached to each joint are defined as in Fig. 2, in which $\mathbf{a_3}$, $\mathbf{b_2}$,

and $\mathbf{c_3}$ represent the rotation direction of q_1, rotation direction of q_2, and translation direction of q_3, respectively. First, for the elbow position given in the reference coordinate frame $\{\mathbf{a_1}\ \mathbf{a_2}\ \mathbf{a_3}\}$, q_3 can be easily obtained as in (4):

$$q_3 = \text{sgn}(\ p_{e.z}) \cdot |\mathbf{p_e}|, \tag{4}$$

where $\mathbf{p_e} = (p_{e,x}\ p_{e,y}\ p_{e,z})$.

Next, the q_1 angle can be calculated as follows. $b_{2,z}$ and $\mathbf{c_2}$ can be readily obtained.

$$b_{2,z} = \sin\ \gamma,\ \ \mathbf{c}_2 = \frac{-\mathbf{p_e}}{|\mathbf{p_e}|} \tag{5}$$

By projecting $\mathbf{b_2}$ onto the $\mathbf{a_1} - \mathbf{a_2}$ plane, the following can also be obtained.

$$b_{2.x}^2 + b_{2.y}^2 = 1 - \sin^{\ 2}\gamma = A \tag{6}$$

In addition, by using the inner product, equation (6) can be rewritten as follows.

$$c_{2,x}b_{2,x} + c_{2,y}b_{2,y} = \cos\ \eta - c_{2,z}\sin\ \gamma = B \tag{7}$$

Then, assuming that $b_{2,y}$ is always positive, we can calculate $b_{2,x}$ and $b_{2,y}$ as shown below. Note that $b_{2,z}$ and $\mathbf{c_2}$ are already obtained above.

$$b_{2,y} = \frac{Bc_{2,y} + \sqrt{B^2c_{2.y}^2 - (c_{2.x}^2 + c_{2.y}^2)(B^2 - Ac_{2.x}^2)}}{c_{2.x}^2 + c_{2b.y}^2}$$
$$b_{2,x} = \frac{B - c_{2,y}b_{2,y}}{c_{2,x}} \tag{8}$$

Consequently, we can obtain q_1, whose range is between $-\pi/2$ and $\pi/2$, as follows.

$$q_1 = \tan^{-1}(-\frac{b_{2,x}}{b_{2,y}}) \tag{9}$$

Finally, the q_2 angle can be obtained as follows. First, we set $\mathbf{p_c^{(2)}}$ and $\mathbf{p_d^{(2)}}$, whose coordinates are given with respect to the $\{\mathbf{b_1}\mathbf{b_2}\ \mathbf{b_3}\}$ coordinate frame as ($\mathbf{p_c^{(2)}} = (0,0,1)$, $\mathbf{p_d^{(2)}} = (0,-\sin\eta/\cos\eta,1)$) on the $\mathbf{b_2}$ -axis and $\mathbf{c_3}$ -axis, respectively. Note that $\mathbf{p_c^{(2)}}$ and $\mathbf{p_d^{(2)}}$ are selected such that $\mathbf{p_c^{(2)}}$ is the projection of $\mathbf{p_d^{(2)}}$ and $|\mathbf{p_d^{(2)}}| = 1$. Then, the coordinate of $\mathbf{p_d}$ with respect to the reference frame becomes

$$\mathbf{p}_\mathbf{d} = -\frac{\mathbf{p_e}}{|\mathbf{p_e}|\cos\ \eta} = R_2^0\mathbf{p}_\mathbf{d}^{(2)}, \tag{10}$$

and because the rotation matrix is orthogonal, we can readily obtain the following:

$$\mathbf{p}_\mathbf{d}^{(2)} = (R_2^0)^T\mathbf{p}_\mathbf{d}. \tag{11}$$

Subsequently, we obtain

$$q_2 = \sin^{-1}(\frac{p_{d.x}^{(2)}}{\sin\ \eta/\cos\ \eta}). \tag{12}$$

Note that q_2 is between $-\pi/2$ and $\pi/2$. With a given elbow position, we can thus derive the solutions for the joint parameters from equations (4), (9), and (12).

D. Analysis of Workspace and Manipulability

On the basis of the forward kinematics, we investigated the workspace of the proposed RCM mechanism. The workspace of the two elbows was calculated from equation (2). The motion ranges of the three joints are $-\pi/3 < q_1 < \pi/3$, $0 < q_2 < \pi/3$, and $0 < q_2 < 200\ mm$.

The workspaces of the mechanism were semi-conical in shape and overlap around the center line. To achieve smooth motion in Cartesian coordinates, we selected the values for the design parameters γ and η so that the elbow workspace could be large and isotropic. By using equation (2) with various sets of design parameters, we studied the size and shape of the elbow workspace (Fig. 3). In this simulation, the range or value of each of the three joints was set to $-\pi/3 < q_1 < \pi/3$, $0 < q_2 < \pi/3$, and $q_3 = 200\ mm$. Note that as q_3 is a constant, we can easily inspect the workspace in the form of a surface. The workspace of the elbow was projected onto the x-y plane (Fig. 3).

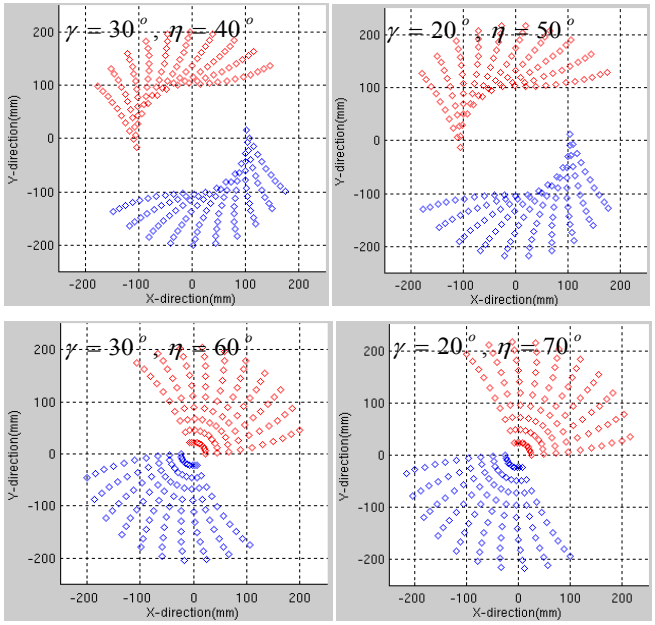

Figure 3. Workspace of elbow for various design parameters

A remarkable observation in the simulation is that the shape of the workspace almost depends on the value of $\gamma + \eta$. The workspace with $\gamma = 30^o$ and $\eta = 60^o$ was similar to that with $\gamma = 20^o$ and $\eta = 70^o$. To identify the conditions for a large workspace, we calculated the area of the blue points shown in Fig. 3, which is proportional to the elbow workspace. Figure 4 shows that the projected area increases with increasing link angle η and decreasing cone angle γ. These conditions are the same as those for high manipulability.

We adopted the determinant of the Jacobian matrix as a measure of manipulability [30]. From equation (2), this measure can be calculated as follows.

$$w = \left| \det \frac{\partial \mathbf{p}_e}{\partial \mathbf{q}} \right| = \left| s_\eta c_\gamma s_{q2} \right| q_3^{\,2} . \qquad (13)$$

For good manipulability, the mechanism should be designed to have a high link angle η and low cone angle γ. Thus, we can satisfy DG3 with good manipulability by selecting a high link angle η and low cone angle γ. In addition, the mechanism will have high manipulability when q_2 and q_3 are far from zero.

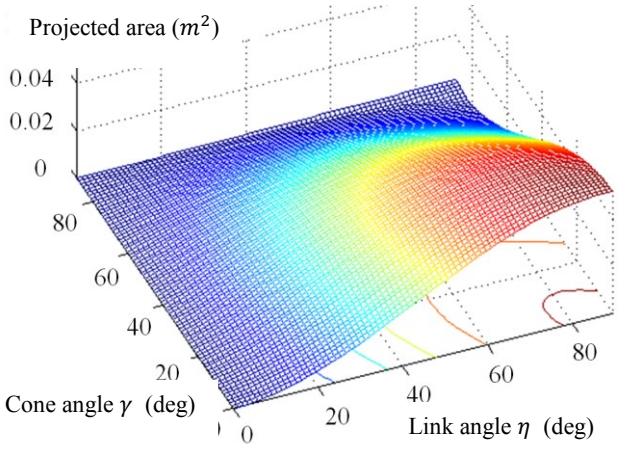

Figure 4. Projected area of the workspace on x-y plane

Next, we established a simulation model to confirm interference among the arms, endoscope, and instruments. With the established model, we checked DG4 and DG5 by superimposing the solid models of the proposed mechanism. This process was performed with various sets of design parameters. For a distance of 4 cm between the two remote centers of the conically shaped RCM mechanisms, we identified the conditions under which the motion areas of the two RCM mechanisms were fully separated. For values of $\gamma + \eta > 90^o$, the mechanisms easily interfered with one another.

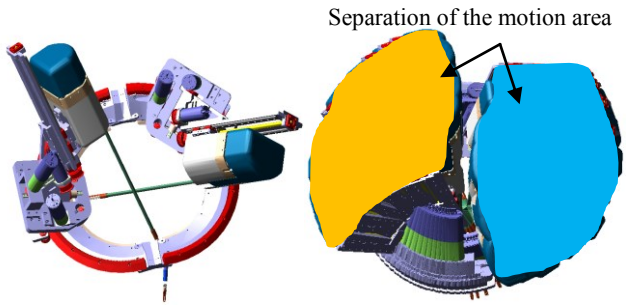

Figure 5. Examination of interference by superimposition.

Among the various sets of values that satisfy the condition $\gamma + \eta \leq 90^o$, we attempted to select a low cone angle γ for a large workspace. However, the base frame of the mechanism is positioned very close to the patient if the cone angle γ is too small (below 30^o). This could pose problems when changes in the orientation and position of the mechanism are required to satisfy various surgical tasks. Thus, we selected $\gamma = 30^o$ and maximized the link angle ($\eta = 60^o$) for the workspace and manipulability. Figure 5 shows the separated motion areas of the two RCM mechanisms.

IV. Fabrication and Performance of the Prototype

In the detailed design process, we focused on a compact design for the RCM mechanism. We roughly estimated the structure, dimensions, and mass properties. We then defined the motion conditions for the elbow. With the established simulation model, we estimated the operation conditions of each joint, including the required torque and force. On the basis of these operation conditions, we selected the motor, gear ratio of the gearhead, lead of the lead screw, and drive mechanism. In this case, the drive mechanism and gearhead were designed for the motor to operate with a speed of around 3000 rpm under nominal operation conditions.

Control of the mechanism was achieved with the inverse kinematics shown in equations (4), (9), and (12). First, the position of the elbow, $\mathbf{p_e}$, was given as a reference position. We then calculated the control references of the joints $\boldsymbol{q}$ from the inverse kinematic relation; therefore, individual joint actuators could be controlled in the joint space to follow the desired trajectory expressed in Cartesian coordinates.

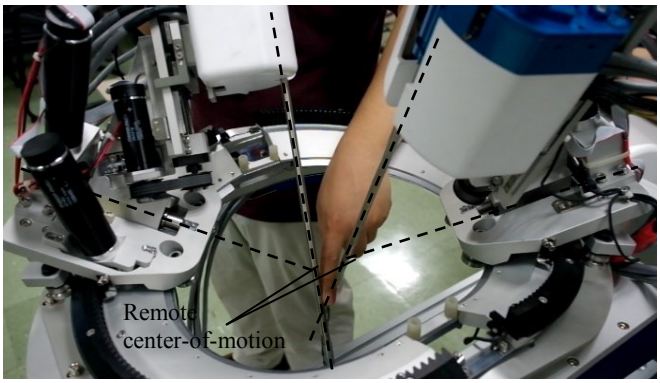

Figure 6. Control experiments showing the remote center motion

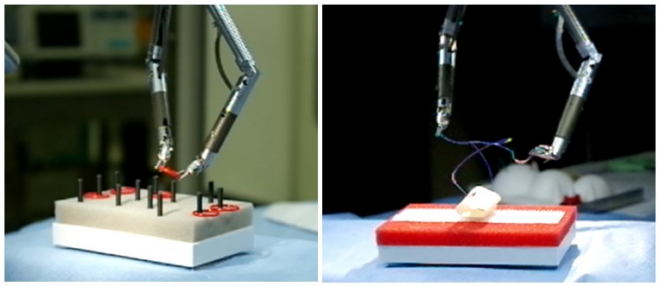

Figure 7. Peg transfer and suturing experiments

The proposed RCM mechanism exhibited motion of the remote center around the incision point (Fig. 6). During the experiment, mechanical interference did not occur between the arms as in the simulation. We also confirmed that the driving modules including the motors have sufficient power for surgical procedures. We tested the Cartesian motion of the elbow under the condition in which a 1-kg mass was applied at the end of the elbow. Within the workspace of the mechanism, smooth motion was observed without sudden divergences or unstable vibrations. Figure 6 shows a finger between the two remote centers. We expect that the endoscope can pass through the area where the finger is inserted.

Finally, a surgical robot equipped with the proposed RCM mechanism successfully performed the peg transfer test and suturing experiment with an externally equipped endoscope. And an in vivo animal trial was performed to verify the design output of conical mechanism[31].

V. Discussion and Future Work

The focus of this study was to design a conically shaped remote center-of-motion mechanism for a single-incision laparoscopic surgery robot. We considered the design goals and showed how the requirements could be satisfied in the design process. We showed that the mechanism maintains a stationary point at the apex of the conical shape.

In addition to the pivot constraints, we prevented collision of the robotic arms in the mechanism by separating their areas of motion. By designing the base frame near an incision point, the mechanism was made to be lighter and more compact, and to require less actuation force. On the basis of the kinematic analysis, the design parameters were determined and the control references of the joints were obtained.

The surgical robot developed in this work will be used to perform in vivo surgical tasks on a porcine model. Although we did not consider the complete surgical system in this study, the results should be considered in designing the system as a whole. The complete surgical system may include two RCM mechanisms, two high-dexterity instruments attached to the end of the proposed mechanism, and an endoscope manipulator. In future studies, we will address the optimal placement of the proposed RCM mechanisms and the endoscope drive mechanism.

References

[1] K. Ahmed, T.T. Wang, V.M. Patel, K. Nagpal, J. Clark, M. Ali, S. Deeba, H. Ashrafian, A. Darzi, and T. Athanasiou, "The role of single-incision laparoscopic surgery in abdominal and pelvic surgery: a systematic review," *Surg Endoscopy*, pp. 1–19, July 2010.

[2] C.R. Tracy, J.D. Raman, J.A. Cadeddu, and A. Rane, "Laparoendoscopic single-site surgery in urology: where have we been and where are we heading?," *Nat Clin Pract Urol*, vol. 5, pp. 561–568, 2008.

[3] J.R. Romanelli, L. Mark, and P.A. Omotosho, "Single port laparoscopic cholecystectomy with the TriPort System: a case report," *Surg Innov*, vol. 15, pp. 223–228, 2008.

[4] A. Gumbs, L. Milone, P. Sinha, and M. Bessler, "Totally transumbilical laparoscopic cholecystectomy," *J Gastrointest Surg*, vol. 13, pp. 533–534, 2009.

[5] S. Kane and K.J. Stepp, "Laparo-endoscopic single-site surgery hysterectomy using robotic lightweight endoscope assistants," *J Robotic Surg*, vol. 3, pp. 253–255, 2010.

[6] M. Piccigallo, U. Scarfogliero, C. Quaglia, G. Petroni, P. Valdastri, A. Menciassi, and P. Dario, "Design of a novel bimanual robotic system for single-port laparoscopy," *IEEE/ASME Trans Mechatron*, vol. 15, no. 6, pp. 871–878, 2010.

[7] J. Ding, K. Xu, R. Goldman, P. Allen, D. Fowler, and N. Simaan, "De sign, simulation and evaluation of kinematic alternatives for insertable robotic effectors platforms in single port access surgery," in *IEEE Int Conf Robotics and Automation*, pp. 1053–1058, 2010.

[8] N. Simaan, X. Kai, W. Wei, A. Kapoor, P. Kazanzides, R. Taylor, and P. Flint, "Design and integration of a telerobotic system for minimally invasive surgery of the throat," *Int J Robotics Res*, vol. 28, pp. 1134–1153, 2009.

[9] D. Abbott, C. Beck, R. Rothstein, and W. Peine, "Design of an endolumenal NOTES robotic system", in *Proc IEEE/RSJ Int Conf Intelligent Robots Systems*, pp. 410-416, 2007.

[10] L. Phee, S. Low, Z. Thant, K. Ho, and S. Chung, "Robotic system for no-scar gastrointestinal surgery," *Int J Med Robotics Comput Assist Surg*, vol. 4, pp. 15–22, 2008.

[11] J.H. Kaouk, R.K. Goel, G.P. Haber, S. Crouzet, and R.J. Stein, "Robotic single-port transumbilical surgery in humans: initial report," *BJU Int*, vol. 103, pp. 366–369, 2009.

[12] G.-P. Haber, M.A. White, R. Autorino, P.F. Escobar, M.D. Kroh, S. Chalikonda, R. Khanna, S. Forest, B. Yang, F. Altunrende, R.J. Stein, and J.H. Kaouk, "Novel robotic da Vinci instruments for laparoendoscopic single-site surgery," *Urology*, vol. 76, no. 6, pp. 1279–1282, 2010.

[13] R. J. Stein, W. M. White, R. K. Goel, B. H. Irwin, G. P. Haber, and J. H. Kaouk, "Robotic laparoendoscopic single-site surgery using gelport as the access platform," *Eur Urol*, vol. 57, no. 1, pp. 132–137, 2010.

[14] P. Berkelman and S. Okamoto, "Compact modular system design for teleoperated laparoendoscopic single site surgery", in *Fourth IEEE RAS/EMBS Int Conf Biomedical Robotics and Biomechatronics,* Roma, Italy, June, pp. 24–27, 2012.

[15] E. Dombre, M. Michelin, F. Pierrot, et al., "MARGE Project: design, modeling and control of assistive devices for minimally invasive surgery", In Proc *Medical Image Computing and Computer-Assisted Intervention* - MICCAI, pp. 1–8, 2004.

[16] O. Schneider and J. Troccaz, "A six-degree-of-freedom passive arm with dynamic constraints (PADyC) for cardiac surgery application: preliminary experiments," *Comput Aided Surg*, vol. 6, pp. 340–351, 2001.

[17] R. Taylor and D. Stoianovici, "Medical robotics in computer-integrated surgery," *IEEE Trans Robotics Automat*, vol. 19, pp. 765–781, 2003.

[18] C.-H. Kuo, J. Dai, and P. Dasgupta, "Kinematic design consideration for minimally invasive surgical robots: an overview," *Int J Med Robotics Comput Assist Surg*, vol. 9, pp. 127–145, 2012.

[19] P. Berkelman and J. Ma, "A compact modular teleoperated robotic system for laparoscopic surgery," *Int J Robotics Res*, vol. 28, no. 9, pp. 1198–1215, September 2009.

[20] D. Sanchez, M. Black, and S. Hammond, "A pivot point arm for a robotic system used to perform a surgical procedure," European Patent No. 1254642, 2002.

[21] J. Hong, T. Dohi, M. Hashizume, et al., "An ultrasound-driven needle-insertion robot for percutaneous cholecystostomy," *Phys Med Biol*, vol. 49, pp. 441–455, 2004.

[22] J. Rosen, J. Brown, L. Chang, et al., "The BlueDRAGON - a system for measuring the kinematics and the dynamics of minimally invasive surgical tools in-vivo," in *Proc IEEE Int Conf Robotics and Automation*, Washington, USA, pp. 1876–1881, 2002.

[23] G.S. Guthart and J.K. Salisbury, Jr., "The intuitive TM telesurgery system: overview and application," in *Proc 2000 IEEE Int Conf Robotics*, pp. 618–621, 2000.

[24] D. Stoianovici, L. Whitcomb, J. Anderson, et al., "A modular surgical robotic system for image guided percutaneous procedures," in *Proc Medical Image Computing and Computer-Assisted Intervention*, Cambridge, MA, USA, pp. 404–410, 1998.

[25] M. Lum, J. Rosen, M. Sinanan, and B. Hannaford, "Optimization of a spherical mechanism for a minimally invasive surgical robot: theoretical and experimental approaches," *IEEE Trans Biomed Eng*, vol. 53, pp. 1440–1445, 2006.

[26] K. Ikuta, K. Sasaki, K. Yamamoto, and T. Shimada, "Remote microsurgery system for deep and narrow space - development of new surgical procedure," in *Proc Medical Image Computing and Computer-Assisted Intervention - MICCAI 2002*, Tokyo, Japan, 25–28 September, pp. 163–172, 2002.

[27] J.S. Navarro, N. Garcia, C. Perez, et al., "Kinematics of a robotic 3UPS1S spherical wrist designed for laparoscopic applications," *Int J Med Robotics Comput Assist Surg*, vol. 6, no. 3, pp. 291–300, 2010.

[28] A.C. Lehman, M.M. Tiwari, B.C. Shah, et al., "Recent advances in the CoBRASurge robotic manipulator and dexterous miniature in vivo robotics for minimally invasive surgery," *Proc IME, Part C: J Mech Eng Sci*, vol. 224, no. 7, pp. 1487–1494, 2010.

[29] M. Lum, C. Friedman, G. Sankaranarayanan, H. King, K. Fodero, R. Leuschke, B. Hannaford, J. Rosen, and M. Sinanan, "The RAVEN: design and validation of a telesurgery system," *Int J Robotics Res*, vol. 28, pp. 1183–1197, 2009.

[30] T. Yoshikawa, "Manipulability and redundancy control of robotic mechanisms," *Int J Robotics Res*, vol. 4, no. 2, pp. 1004–1009, 1985.

[31] H. Kim, et al "A novel compact single incision surgical robot with conical remote center-of-motion mechanism and rod elbow joint," in *EUS Annual Meeting*, San Diego, USA, May, p 25, 2013.